Age-Related Changes in HAPLN1 Increase Lymphatic Permeability and Affect Routes of Melanoma Metastasis

Brett L. Ecker[#,1,2], **Amanpreet Kaur**[#,2,3], **Stephen M. Douglass**[2], **Marie R. Webster**[2], **Filipe V. Almeida**[2], **Gloria E. Marino**[2,4], **Andrew J. Sinnamon**[1], **Madalyn G. Neuwirth**[1], **Gretchen M. Alicea**[2,3], **Abibatou Ndoye**[2,3], **Mitchell Fane**[2], **Xiaowei Xu**[5], **Myung Shin Sim**[6], **Gary B. Deutsch**[7], **Mark B. Faries**[8], **Giorgos C. Karakousis**[1], and **Ashani T. Weeraratna**[2,**]

[1]Department of Surgery, University of Pennsylvania, Philadelphia, PA

[2]The Wistar Institute, Philadelphia, PA

[3]University of the Sciences, Philadelphia, PA

[4]Perelman School of Medicine, University of Pennsylvania, Philadelphia, PA

[5]Department of Pathology, University of Pennsylvania, Philadelphia, PA

[6]The University of California, Los Angeles, CA

[7]Northwell Health Institute, Los Angeles, CA.

[8]The Angeles Clinic and Research Institute, Cedars Sinai, Los Angeles, CA

[#] These authors contributed equally to this work.

Abstract

Older melanoma patients have lower rates of sentinel lymph node (LN) metastases yet paradoxically have inferior survival. Patient age correlated with an inability to retain Technetium radiotracer during sentinel LN biopsy in over 1000 patients, and high technecium counts correlated to better survival. We hypothesized that loss of integrity in the lymphatic vasculature due to ECM degradation might play a role. We have implicated HAPLN1 in age-dependent ECM degradation in the dermis. Here we queried whether HAPLN1 could be altered in the lymphatic ECM. Lymphatic HAPLN1 expression was prognostic of long-term patient survival. Adding rHAPLN1 to aged fibroblast ECMs *in vitro* reduced endothelial permeability via modulation of VE-Cadherin junctions, whereas endothelial permeability was increased following HAPLN1-knockdown in young fibroblasts. In vivo, reconstitution of HAPLN1 in aged mice increased the number of LN metastases, but reduced visceral metastases. These data suggest that age-related changes in ECM can contribute to impaired lymphatics.

Keywords

angiogenesis; lymphangiogenesis; metastasis; melanoma; aging

To Whom Correspondence Should Be Addressed: Ashani T. Weeraratna, The Wistar Institute, Rm 452/ 454A, 3601 Spruce Street, Philadelphia, PA 19104. Phone: 215-495-6937; Fax: 215-495-6938, aweeraratna@wistar.org.

Introduction:

The progression of cancer to distant metastatic sites is the single most prognostic factor for many solid organ malignancies (1, 2). In the specific case of cutaneous melanoma, increasing age identifies a high-risk group (3), with more frequent development of incurable visceral metastasis (4). The prognostic role of age, and its impact on the clinical course of melanoma, is unlikely to be fully explained by differences in the primary tumor, as elderly patients demonstrate shorter disease-specific survival even when adjusting for known pathologic variables (3, 4). The biological effects of aging on patterns of tumor dissemination have been largely unexplored. Whether age-related changes in tumor phenotype drive lymphatic versus hematogenous metastasis has important clinical implications, as regional lymphatic metastases are frequently treated with surgical resection, whereas distant metastases are often incurable. Clinical observation supports initial melanoma spread through the intradermal lymphatics to regional nodal basins, with subsequent progression to distant sites (5). Tumor invasion into the lymphatic conduit allows passage to regional lymph nodes, which are secondary immune organs that function to filter lymph by containing antigens and providing a context for antigen presentation to immune cells (6). In the absence of distant metastases, nodal involvement is the most prognostic factor for survival. Current National Comprehensive Cancer Network (NCCN) guidelines support the use of sentinel node biopsy (SNB) to evaluate the tumor status of the regional lymphatic drainage basin in patients with clinically localized melanoma. However, recent data have shown that lymph node dissection did not increase melanoma-specific survival among melanoma patients (7). Notably, older patients demonstrate a lower incidence of SNB metastases – which should confer a more favorable prognosis – yet paradoxically have inferior disease-specific survival compared with younger patients(8, 9), which cannot be simply explained by age related changes in the false negative results of SNB(9). No biologic mechanism has yet been identified that accounts for this clinical observation.

We have previously demonstrated that changes in the aging tumor microenvironment, such as secreted factors from dermal fibroblasts, can promote melanoma invasion and may account for inferior age-dependent clinical outcomes. In our analysis of the young and aged fibroblast secretome, the most highly secreted protein by young fibroblasts is the hyaluronan and proteoglycan link protein 1 (HAPLN1) (10), which crosslinks hyaluronan to the extracellular matrix (ECM). Hyaluronan alters the ability of fibroblasts to contract collagen matrices(11) and its role in cancer is believed to be tissue specific; reduced hyaluronan is associated with increased tumorigenesis in normally hyaluronan-rich tissues such as skin(12). Our recent data show that HAPLN1 loss in the aged tumor microenvironment drives a breakdown in the crosslinking of the ECM, which promotes melanoma migration while limiting intravasation of tumor-infiltrating lymphocytes (13).

In patients with tumors, alterations in permeability of regional lymphatic channels, may contribute to impaired flow of lymphatic fluid. In order to maintain a strong, directional lymphatic flow, lymphatic vessels rely upon tight connections between the endothelial cells of which they are composed. These connections, in turn, rely upon stabilization by a scaffold of extracellular matrix, secreted by fibroblasts, and made up of fibrillar collagen(14). It has

been shown that during aging lymphatic vessels are susceptible to permeability and degradation, affecting lymphatic transport(15). We hypothesized that age-dependent loss of lymphatic endothelial integrity may also functionally impair the lymphatic system's capacity to contain tumor cells, allowing them to escape from lymph nodes to distant sites. We further hypothesized that the age-related changes in ECM, similar to those we see in the skin, might affect lymphatic vessel permeability. Here, we report a novel role of the HAPLN1 loss in the aging lymphatic ECM in mediating lymphatic endothelial permeability, thus permitting melanoma cells to escape from the lymphatic system to distant metastatic sites. Such observations have important implications for the surveillance and treatment of melanoma in an aging population.

Results:

Age determines patterns of melanoma dissemination

Consecutive American Joint Committee on Cancer [AJCC] Stage I-II melanoma patients underwent SNB using Technetium (^{99m}Tc) radiotracer (n=1081). SNB is a technique for the staging of subclinical regional metastatic disease using lymphatic mapping. ^{99m}Tc injected into the peritumoral skin is transported by dermal lymphatics on a direct pathway from the cutaneous site to the drainage lymph nodes (i.e., "sentinel" node). The sentinel node is subsequently identified in the operating room using a hand-held gamma probe and surgically resected. There was a significant correlation with increasing age and lower ^{99m}Tc counts in the sentinel node (Figure 1A, n=1081 patients, Spearman's ρ=−0.30, p<0.001), despite standardized injection protocols of radiotracer at the site of melanoma. Impaired retention of ^{99m}Tc was evident by decreased signal intensity in corresponding lymphoscintigraphy images (Figure 1B). Patients provided written informed consent for the procedure. De-identified medical records were used to generate the analyses used in the paper and an exemption determination from IRB review was independently granted.

Decreased radiotracer counts may signify increased permeability through the lymphatic system and/or decreased transport to the draining lymph node. Aging is associated with decreases in the contraction frequency of lymphatic collectors, reducing lymph velocity (15, 16). Thus, patients with SNB which are negative for metastases may have (1) early stage disease that has not spread to the regional lymphatics (i.e., true negatives), (2) permeable lymphatics that allow for tumor migration through the SNB to reach the systemic circulation (i.e., false negative), or (3) tumor that cannot reach the lymph node due to faulty lymphatics. In accordance with our hypothesis that this loss of dye retention corresponded to both an inability to get to the lymph node (due to permeability issues) as well as an inability to be retained in the lymph node due to permeability of the lymph node capsule, rather than decreased rates of lymph node metastasis, survival (adjusted for number of positive lymph nodes, ulcerations and T-stage classification) was actually improved for patients who had higher than median levels of ^{99m}Tc in their lymph nodes (Figure 1C, HR 0.831, p=0.0014, 95% CI 0.719-0.92). Multivariable analyses of these data in a multivariate Cox model, accounting for stage is shown as Supplemental Table 1.

Given that aging appeared to be associated with increased SNB permeability, we hypothesized that older patients with negative SNB (i.e., no evidence of lymphatic

metastases) would have a higher rate of distant, visceral metastasis. The distant metastatic-free survival (DMFS) was analyzed in an institutional series of 1,649 patients who underwent negative SNB (i.e., AJCC pStage I-II melanoma). Older age was associated with significantly shorter DMFS (mean [95% CI]: 15.9 [15.2-16.6] years vs. 18.4 [17.7-19.0] years, log rank p<0.001; Figure 1D). Moreover, in a multivariate Cox proportional hazards model adjusting for known prognostic factors (e.g., Breslow depth and the presence of ulceration and lymphovascular invasion), older age remained independently associated with a higher risk of distant recurrence (HR 1.49, 95% CI 1.01-2.20) (Supplemental Table 2).

Next to determine if we could experimentally recapitulate these data, mCherry labeled Yumm1.7 cells, derived from the Braf^{V600E}/Cdkn2a$^{-/-}$/Pten$^{-/-}$ mouse model of melanoma(17), were injected into the dermis of young (8 weeks) or aged (52 weeks) C57/BL6 mice and tumor burden in the draining inguinal lymph node and the lungs was quantified after 5 weeks. Tumor cells were identified by positive immunhistochemical staining for mCherry, which is specific for the mCherry labeled Yumm1.7 cells. As with the human epidemiologic studies, the aged mice had reduced lymph node metastases but increased tumor burden in the lung (Figure 1E, F). Together these data confirm that aging increases visceral metastatic dissemination despite reduced lymphatic metastasis.

HAPLN1 loss in the aged microenvironment contributes to ECM changes leading to loss of lymphatic vessel integrity.

We hypothesized that changes in lymphatic architecture underlie age-related changes in lymphatic permeability, both of the lymphatic vessel and the lymph node itself. Melanoma cells travel via afferent lymphatic vessels to enter the subcapsular sinus of lymph nodes(18). The lymphatic vessels are embedded in fibroblast-secreted ECM, where lymphatic vessel integrity is maintained by the cell-cell contact between the endothelial cells that make up the lymph vessels, as well as the anchoring of these cells to the ECM, which further stabilizes the connection. To test this, lymph node specimens available in the TCGA from young (<50 years) and aged (>50 years) melanoma patients were used to perform GSEA analysis for ECM fibril organization, where the signature showed significant enrichment in young lymph nodes relative to the aged lymph node samples (Figure 2A, p=0.008). To explore age-related differences in matrix orientation *in vitro*, lymphatic fibroblasts isolated from young or aged human donors were used to prepare matrices and analyzed for fibronectin fiber orientation, and compared to matrices made by dermal fibroblasts from young and aged human donors. Similar age-related decreases in matrix complexity were observed in both dermal and lymphatic (Figure 2B-C) fibroblast matrices, supporting previous observations of the broad similarities between fibroblasts of these two anatomic sites (19).

In order to determine whether age-dependent structural changes in the ECM impact on endothelial permeability, acellular matrices produced *in vitro* by young or aged fibroblasts in transwells were reconstituted with an endothelial (HUVEC) monolayer and dextran-conjugated Texas Red fluorescent dye was added to the upper chamber (see schematic in Figure 2D). HUVEC cells were utilized after initial failures to reliably grow lymphatic endothelial cells in vitro. The integrity of the endothelial cell monolayer was determined with spectrophotometry by measuring the concentration of Texas Red that had diffused into

the bottom well after 30 minutes. There was significantly increased endothelial permeability in the context of the aged fibroblast matrix in multiple cell lines (Figure 2E). These data support the concept that changes in the aged ECM can de-stabilize lymphatic vessel integrity, leading to increased permeability.

Previous work from our lab has demonstrated an age-dependent loss of fibroblast-secreted HAPLN1 in the skin, which in turn impairs ECM structure and accelerates melanoma invasion (13). To determine whether HAPLN1 could contribute to the observed age-related changes in lymphatic vessel permeability, the transwell permeability assay was performed using an aged fibroblast cell line treated with increasing concentrations of rHAPLN1. The treatment of aged fibroblasts with rHAPLN1 showed increased matrix complexity (Figure S1A). When produced in transwells and reconstituted with endothelial cells, we observed a step-wise decrease in endothelial permeability (Figure 2F, second cell line in Figure S1B). Likewise, endothelial cells plated on an acellular ECM produced by young fibroblasts following HAPLN1 knockdown (Figure S1C) lost matrix complexity (Figure S1D) and subsequently evidenced a significant increase in endothelial permeability (Figure 2G). Next, to see if melanoma cells could more easily transverse the barriers created by aged vs. young fibroblasts, we labeled melanoma cells, plated them atop endothelial cells attached to matrices laid down by young or aged fibroblasts in which HAPLN1 had been manipulated, and then measured the velocity of the tumor cells. In the presence of HAPLN1-containing matrices, tumor cells were less able to cross the endothelial cell barrier (Figure 2H). These data suggest that HAPLN1 loss during aging, which we have previously shown destabilizes the ECM, can contribute to lymphatic permeability.

Endothelial cell-cell adhesion mediates permeability of aged lymphatic matrix

We next assessed whether changes in lymphatic permeability might be explained by differences in cell-cell adhesion due to ECM degradation. VE-cadherin is a critical component of endothelial adherens junctions and mediates vessel permeability (20). Endothelial cells were plated on acellular matrices following extraction of young or aged fibroblasts, and VE-cadherin expression was assessed by immunofluorescence. HUVECs on a young fibroblast matrix evidenced strong VE-cadherin membrane staining with a zipper-like appearance between neighboring cells, which was reduced in endothelial cells plated on an aged fibroblast matrix (Figure 3A, B; Additional lines, Figure S2A, B). There was also reduced immunofluorescence signal in the aged context, suggesting such structural changes were related to reduced cell surface protein (Figure 3A,B). As the knockdown of HAPLN1 in young fibroblasts or the additional of rHAPLN1 to aged fibroblasts was sufficient to change endothelial permeability in a transwell assay, we next investigated whether such changes would alter VE-cadherin signaling. The treatment of fibroblasts from aged donors with rHAPLN rescued HUVEC endothelial adherens junctions, where VE-cadherin signaling was comparable to that observed in the context of young fibroblasts. Additionally, the knockdown of HAPLN1 in young fibroblasts reduced the complexity and overall expression of VE-cadherin in the HUVEC monolayer (Figure 3A,B; Figure S2C,D).

Lymphatic endothelial permeability is also dependent on anchorage to the ECM by integrin protein complexes(15). HUVECS were plated on acellular matrices following extraction of

multiple young or aged fibroblasts and the relative mRNA expression of integrin subunits (α1, α5, β1, β5) and CD44 was assessed by qPCR. HUVEC expression of α1 and β1 integrins was significantly reduced in the aged matrix relative to the ECM produced by young fibroblasts (Figure 3C). Moreover, endothelial cells plated onto a matrix produced by two different knockdown shHAPLN1 young fibroblasts had reduced integrin expression (Figure 3D), supporting a causal role for HAPLN1-mediated ECM complexity and endothelial integrity.

To explore the role of endothelial cell adhesion *in vivo*, human SNB specimens were co-stained for VE-cadherin and podoplanin by immunohistochemistry. Patients provided written informed consent for the procedure, and de-identified samples were obtained under exemption. Podoplanin is a specific lymphatic endothelial glycoprotein that is not expressed in blood vessel endothelium (21). In aged patients, there was a near absence of VE-cadherin staining (pictured in red; Figure 3E) in the lymphatic channels identified (pictured in brown). In contrast, lymphatic channels in the SNB specimens from young patients evidenced frequent co-localization of podoplanin with VE-cadherin, where channels appear pink, and this is quantitated. These data confirm the age-dependent loss of VE-cadherin in lymphatic endothelium that may underlie observed changes in permeability.

HAPLN1 loss during aging affects permeability of the lymph node sinus as well as the lymphatic vasculature.

The subcapsular sinus, lined by lymphatic endothelial cells, regulates tumor motility through the lymph node (22). Since the subcapsular sinus is continuous with the endothelium of the afferent lymph vessels, we hypothesized that similar age-related changes would be present in the lymph nodes, and may account for differences in their function to contain metastatic cells and prevent dissemination to visceral sites. Staining of the young and aged mouse lymph nodes for fibronectin demonstrated a loss of fibronectin in the stroma around the lymph node capsule of aged mice (Figure 4A). We asked whether, as with the previous observations above, this could be due to changes in HAPLN1 levels. HAPLN1 expression was significantly lower in the aged murine lymph nodes (Figure 4B). To study the impact of HAPLN1 *in vivo*, inguinal lymph nodes from aged C57/BL6 mice were treated with rHAPLN1 and their collagen architecture was evaluated using two-photon microscopy. Treatment increased the ECM complexity of the lymphatic pericapsular space (Figure 4C). Using anisotropic/ isotropic quantification of fiber alignment, we also saw that loss of matrix complexity with age (Figure 4D) could be reverted by treatment with HAPLN1 (Figure 4E, Figure S3A). This in turn restored VE-cadherin staining in regions of lymphatic endothelium (Figure S3B). Similarly in patient samples, there was evidence of reduced HAPLN1 in the sentinel lymph nodes of aged melanoma patients, both at the protein (Figure 4F) and transcriptomic (Figure 4G) level.

To evaluate the association between HAPLN1 expression and lymphatic permeability *in vivo*, the Geiger counts corresponding to the sentinel lymph nodes of melanoma patients (n=86) were correlated with HAPLN1 immunohistochemical staining. Patients provided written informed consent for the procedure, and de-identified samples collected under an IRB exemption were used. A total of 21 (23.3%) patients had HAPLN1-positive SLNs. The

Geiger counts of HAPLN1 positive SLNs were significantly higher than those without any HAPLN1 staining (median [IQR]: 2364 [1079-3235] counts/sec vs. 2123 [831-1667] counts/ sec; p=0.005). Because of the potential bias of age on HAPLN1 expression, the analysis was repeated in the older (age >50 years) patient subset, where a similar relationship between higher HAPLN1 and increased radiotracer retention was observed (1782 [883-2754] counts/sec vs. 772 [260-1967] counts/sec; p=0.034, Figure 4H)

Given these findings, we hypothesized that differences in HAPLN1 expression in the regional lymph nodes of melanoma patients would have prognostic significance for long-term survival. Using a subset of non-metastatic melanoma patients where regional lymphatic tissue was included in the TCGA database (n=192), we observed a threshold effect of improved overall survival associated with the upper quartile of HAPLN1 expression (log rank p<0.001; Figure 4I), with similar long-term outcomes observed in the lower three quartiles of mRNA expression (Figure S4). Given potential confounding effects of age on this association, the prognostic value of HAPLN1 expression was confirmed in a multivariate Cox proportional hazards model, which controlled for both AJCC stage and patient age (Table 1). Taken together, these data indicate that loss of HAPLN1 during aging can destabilize the ECM, which in turn can affect the VE-cadherin connections between the lymphatic endothelial cells, and increase permeability of the both the vessels and the nodes.

HAPLN1-dependent lymph node permeability determines melanoma progression

To determine if HAPLN1-mediated permeability would be sufficient to change the patterns of metastasis, the draining lymph nodes of aged C57/BL6 mice were treated with rHAPLN1 or PBS control preceding heterotopic tumor cell injection. In contrast to prior experiments where *peritumoral* injection of rHAPLN1 into aged mice reduced the size and metastatic potential of primary tumors (13), *lymphatic* injection of rHAPLN1 (into the draining lymph nodes) had no effect on tumor size (Figure S5A), which may be expected given its local effects of collagen matrix orientation. We hypothesized that HAPLN1 treatment of aged lymph nodes would decrease lymphatic permeability and thereby decrease the rate of distant metastasis. In support, aged mice treated with rHAPLN1 had greater rates of lymphatic micrometastases (Figure 5A) as well as greater lymphatic tumor burden, suggesting decreased "escape" from the draining lymph node (Figure 5B-C). While lymph node metastases are associated with an unfavorable prognosis for melanoma patients, surgical resection of locoregional disease (i.e., the primary site and the draining lymphatic basin) is often an effective treatment not typically available to patients with disease progression to visceral sites. Hence, the containment of tumor metastasis to lymphatic basins may have therapeutic implications. Accordingly, rHAPLN1 treatment of draining lymph nodes in this mouse cohort led to a *reduced* frequency of distant pulmonary micrometastasis despite higher rates of lymphatic metastasis (Figure 5D-E). There were no differences in primary tumor angiogenesis that may have provided an alternative (non-lymphatic) pathway for visceral metastatic spread (Figure S5B-C). Such observations support the hypothesis of sequential progression of melanoma tumor cells through the lymphatic system to visceral sites, and the role of HAPLN1-mediated ECM integrity in regulating lymphatic permeability (summarized in Figure 6).

Discussion:

Melanoma patients of older age experience a higher rate of distant metastasis and inferior overall survival. In particular, the dissemination of melanoma cells beyond the primary site and regional lymphatic basin that are the primary targets for surgical extirpation, presents a clinical dilemma with poor therapeutic options. While the relationship between age and sentinel lymph node positivity has been previously described, herein we identify (1) age-related alterations in the perilymphatic extracellular matrix that mediates lymphatic permeability via destabilization of VE-Cadherin junctions, and (2) a novel role of HAPLN1 in lymphatic ECM integrity, including its prognostic role in human patients and its potential therapeutic value in reducing visceral metastases.

Age-dependent loss of ECM integrity has been demonstrated in studies of skin, and we have recently determined its impact on primary melanoma tumor activity (13). Whether similar age-related degradation occurs in stroma surrounding lymphatic vessels and nodes has rarely been studied. In one previous analysis of mesenteric lymphatic vessels isolated from young and aged rats, aging was associated with a decrease in gap junction proteins and the thickness of the endothelial cell glycocalyx, as well as increased hyperpermeability to bacterial pathogens(15). Our data confirm similar changes in lymphatic endothelial gap junctions and integrins in both *in vitro* lymph vessel constructs and *in vivo* lymph node biopsies from melanoma patients and mice. Moreover, age-related changes in lymphatic endothelium were sufficient to mediate permeability in transwell assays using human cell lines as well as in melanoma patients receiving technetium dye for sentinel lymph node detection. Notably, in these studies utilizing mouse and human tissues, the lymph nodes were studied separately from the afferent lymphatic vessels (that transport tumor cells from the primary tumor site in the dermis) due to technical limitations of the models and availability of tissues. Unfortunately, this prohibited the specific study of the effects of aging on dermal lymphatic vessels apart from the draining lymph nodes *in vivo*. However, given the greater rates of in-transit metastasis that develop in older melanoma patients, we hypothesize that similar changes in permeability occur in the dermal lymphatic vessels (Figure 6). New techniques will be needed to explore the effects of aging on collecting dermal lymphatics and their role in mediating in-transit disease.

Second, the identification of age-related loss of lymphatic HAPLN1 provided a prognostic biomarker and potential therapeutic target. The loss of HAPLN1 with aging was demonstrated at both the protein and gene expression level. Importantly, patients with high lymphatic HAPLN1 expression were 56% less likely to die, regardless of age and disease stage. The prognostic utility of HAPLN1 as assessed by IHC, which could be more readily incorporated into current clinical practice, remains to be determined. Nevertheless, the targeting of aged lymph nodes with rHAPLN1 *in vivo* was sufficient to change lymph node architecture and abate the development of visceral metastasis. HAPLN1 – and possibly similar ECM-associated proteins – can be targeted to reduce the rates of visceral metastasis. At a minimum, incorporation of HAPLN1 expression, particularly in elderly melanoma patients with negative sentinel lymph node biopsies, into clinical algorithms guiding postoperative surveillance and adjuvant systemic therapy may improve the management of those patients at greatest risk for the development of visceral metastasis.

By inference, these data support the sequential progression model of tumor metastasis – whereby tumor spreads from primary site, to lymph node, and then to distant visceral sites. The sequential cascade model is supported by clinical observation, particularly that the development of lymphatic disease often precedes distant metastasis(23, 24). Yet the lack of survival benefit following lymphadenectomy in melanoma patients has inspired the alternate view that lymphatic and visceral metastasis develop independently(25). However, these two observations can be reconciled upon recognition that lymphadenectomy can only improve survival if performed prior to tumor spread from the lymph nodes to distant sites. In our experiments, young mice or aged mice treated with lymphatic rHAPLN1 had increased lymphatic metastasis and concurrently decreased pulmonary metastasis, providing direct causal support for lymphatic dissemination preceding hematogenous spread. However, the timing of cancer cell trafficking in this cascade is not known, and likely varies by primary tumor burden, disease site and host-related factors. Still, the removal of lymph nodes at an early stage prior to spread beyond the regional basin would likely be curative. Alternatively, strategies to improve lymphatic integrity prior to lymphadenectomy may decrease the false negative rate of sentinel lymph node biopsy and improve long-term survival.

While lymphatic metastasis is the dominant pattern of tumor dissemination in melanoma patients, peritumoral angiogenesis may provide an alternative pathway for tumor egress that bypasses the lymphatic system altogether. Our previous work identified secreted frizzled-related protein 2 (sFRP2) as an age-dependent component of the fibroblast secretome (26), and sFRP2 promotes angiogenesis via activation of the Wnt/Ca^{2+} signaling pathway (27). Moreover, the targeting of sFRP2 in breast tumor endothelium inhibits tumor angiogenesis and growth(27). In direct support, aged mice have higher expression of sFRP2 than young mice are more likely to develop tumors with a higher density of CD31-positive vessels (26), providing a mechanism by which tumor cells may reach visceral sites independent of the age-related changes in lymphatic permeability. These are not mutually exclusive observations: indeed the aged tumor microenvironment may promote visceral metastasis by multiple mechanisms that lead to inferior clinical outcomes in melanoma patients. Still, the decrease in visceral metastasis simultaneous with the increase in lymphatic metastasis observed in these experiments following the treatment of lymph nodes (and not the primary tumor or peritumoral lymphatics) with rHAPLN1 highlights the causal role for lymph node permeability in mediating melanoma dissemination.

In conclusion, these data suggest that aging leads to degradation of the perilymphatic stroma, which alters lymph node permeability and dictates the route of metastasis. Age should be an important consideration in the management and treatment of melanoma patients, and requires specific strategies to improve outcomes for this growing high-risk patient population.

Methods:

Cell lines and culture conditions

Dermal fibroblast cell lines were obtained from Biobank at Coriell Institute for Medical Research. Human lymphatic fibroblasts were isolated from lymph nodes from young (<35 years) and aged (>50 years) human donors by ScienCell Research Laboratories (Carlsbad,

CA) and characterized by their spindle-shaped morphology and fibronectin-positive staining. The fibroblasts were cultured in DMEM (Invitrogen) supplemented with 10% FCS and 4mM L-Glutamine. HUVEC cells were obtained from Lonza and cultured in EGM-2MV media (CC-3202, Lonza). Yumm1.7 murine melanoma cells were cultured in DMEM supplemented with 10%FCS and 4mM L-Glutamine. 1205lu melanoma cells were maintained in DMEM supplemented with 5%FCS and 4mM L-Glutamine and cultured at 37°C in 5% CO_2 and medium was replaced as required. Short tandem repeat profiling was done for melanoma cells and compared against our internal control of over 200 melanoma cell lines as well as control lines such as HeLa and 293T and the results are available upon request. Mycoplasma testing was carried out using a Lonza MycoAlert assay at the University of Pennsylvania Cell Center Services.

Lentiviral production and infection

HAPLN1 shRNA was obtained from the TRC shRNA library available at The Wistar Institute (TRCN0000150501, TRCN0000153400). Sequencing based verification of all plasmids was performed at the Genomics facility at The Wistar Institute. Lentiviral production was performed according to the protocol suggested by the Broad Institute. Briefly, 293T cells are plated at 70% confluency and co-transfected with shRNA plasmid and the lentiviral packaging plasmids (pCMV-dR8.74psPAX2, pMD2.G). pLKO.1 empty vector was used as a control. For transduction, cells were treated with lentivirus overnight and allowed to recover for 24 hours before selection using puromycin (1μg/ml).

Lymphoscintography

Count data was collected as part of standard of care. The data were not collected as part of a prospective clinical trial. Patients provided written informed consent for the procedure. De-identified medical records were used to generate the analyses used in the paper and an exemption determination from IRB review was independently granted (FARM-SLNRETRO-0805). Sentinel lymph node biopsy was routinely performed per institutional standard protocols, using radiotracer dye with or with vital blue dye. Lymphoscintigraphy was typically performed after radiotracer dye injection at the site of the primary and a hand-held gamma probe was used intra-operatively to assist with identification of the lymph nodes with radiotracer uptake. More specifically, one mCi total of filtered Technetium-99m sulfur colloid was injected intradermally in 4 separate aliquots (0.1-0.2 mL each) surrounding the melanoma. A gamma camera with low energy parallel hole collimator was utilized to obtain static emission images of the injection site as well as transmission images of the sentinel node. To aid in the operative identification of the SLN, isosulfan blue dye (Lymphazurin; Tyco Healthcare, Norwalk, Connecticut, USA) (1%, 1–3ml/case) was injected prior to skin incision. A hand-held gamma probe (C-Trak; Care Wise Medical Products Corporation, Morgan Hill, California, USA) was used to localize the sentinel node on the basis of accumulation of the Tc-99m sulfur colloid, where >10% of background counts was considered positive. The maximum counts of each lymph node were confirmed *ex vivo* following surgical removal.

Immunohistochemistry

Patient samples were collected under IRB exemption approval (protocol EX21205258-1). FFPE sections were deparaffinized using xylene followed by rehydration through series of alcohol washes and finally PBS. Heat-mediated antigen retrieval was performed using citrate based retrieval buffer (Vector Labs, H-3300). Samples were blocked in peroxide blocking buffer (Thermo Scientific), followed by protein block (Thermo Scientific) and incubated in appropriate antibody at 4°C overnight in a humidified chamber. Following day, samples were washed and incubated with a biotinylated secondary antibody (Thermo Scientific) followed by Streptavidin-HRP incubation. Samples were then washed in PBS and incubated in 3-amino-9-ethyl-1-carboazole (AEC) chromogen and counterstained with Mayer's hematoxylin, rinsed in dH_2O and mounted in aquamount. For mouse samples to be incubated with mouse antibodies, samples were blocked for an additional hour with mouse on mouse block (MKB-2213, Vector Labs). Multiplexed IHC samples were developed initially with DAB chromogen (Thermo Scientific) followed by blocking with protein block and incubation with second primary antibody developed using AEC chromogen. Primary antibodies used were as follows, mCherry (1:500, NBP2-25157, Novus Biologicals), HAPLN1 (1:100, TA325115, Origene), podoplanin (1:100, 322M-14, Sigma Aldrich), VE-cadherin (1:50, MAB9381, R&D Systems), Lyve-1 (1:50, ab14917, abcam), CD31 (1:50, ab28364, abcam).

Immunofluorescence

Samples were fixed in 4% paraformaldehyde for 20 minutes followed by 1 hour treatment with blocking buffer (0.2% each of triton-x, BSA, gelatin and casein and 0.02% Sodium azide). Cells were incubated in primary antibody and incubated overnight at 4°C. Following day, cells were washed in PBS and incubated with appropriate secondary antibodies (Alexa fluor series, Invitrogen, 1:2000) at room temperature for 1 hour. Cells were washed in PBS, incubated with DAPI (Invitrogen, 1:10,000) and mounted in Prolong Gold anti-fade reagent (Invitrogen). Images were captured on a Leica TCS SPII scanning laser confocal system. Primary antibodies used were as follows, Fibronectin (1:200, #F3648, Sigma Aldrich), VE-cadherin (Human: 1:50, MAB9381, R&D Systems; Mouse: 1:10, 138001, Biolegend), Lyve-1 (1:50, ab14917, abcam).

Quantitative PCR

mRNA was harvested using phenol-chloroform method as described previously and cleaned using RNeasy mini kit (Qiagen). HUVECs were plated on fibroblast-derived matrices for 24 hours and harvested using Trizol. For the murine inguinal lymph nodes, they were harvested, freshly digested in Trizol, and homogenized (X). Samples were then mixed with chloroform and clear layer was collected and processed through RNA cleanup kit using manufacturer's protocol. RNA concentration was measured using Nanodrop 2000 (Thermo Scientific). One microgram of RNA was used to prepare cDNA using iscript cDNA synthesis kit (1708891, Bio-rad). cDNA was diluted 1:5 before use. Each 20μl reaction comprised 1μl Power SYBR Green Master Mix (4367659, Invitrogen), 1μl primer mix (Final concentration 0.5μM) and 1μl cDNA. Standard curves were generated for each primer and used to perform relative quantification. All samples were normalized to 18S primer pair (AM1718, Invitrogen).

Primer sequences were obtained from IDT (Coralville, Iowa) for ITGA1 (forward – GTGCTTATTGGTTCTCCGTTAGT, reverse – CACAAGCCAGAAATCCTCCAT), ITGA5 (Forward – GCCTGTGGAGTACAAGTCCTT, reverse – AATTCGGGTGAAGTTATCTGTGG), ITGB1 (Forward – GCCGCGCGGAAAAGATG, reverse – ACATCGTGCAGAAGTAGGCA), ITGB5 (Forward – TCTCGGTGTGATCTGAGGG, reverse – TGGCGAACCTGTAGCTGGA), CD44 (Forward – AATGCCTTTGATGGACCAAT, Reverse - TAGGGTTGCTGGGGTAGATG), HAPLN1(Forward – TCACACAAAGGACCAGAATCG, Reverse – TGGTAATCTTGAAGTCTCGAAAGG).

Preparation of fibroblast matrices

Fibroblast matrices were prepared as previously described(28). Briefly, in a 24 well plate, 12mm coverslips (No.1) were added and coated with 0.2% gelatin solution for 1 hour. Wells were washed with DPBS (without Ca^{2+} and Mg^{2+}), followed by treatment with 1% glutaraldehyde for 30 minutes at room temperature. After washing with DPBS, coverslips were incubated with 1M ethanolamine for 30 minutes at room temperature. Coverslips were washed with DPBS and 1×10^5 fibroblasts were plated on the coverslips and incubated overnight at 37°C, 5% CO_2. Following day, fresh media containing 50μg/ml L-ascorbic acid was added to the wells. L-ascorbic acid was added daily to the wells with fresh media replacement every other day. rHAPLN1 (#2608-HP, R&D Systems) was added to the media at varied concentrations and replaced during media changes. Matrices were harvested after a total of 5 treatments and analyzed as described under various sections.

Anisotropic analysis of fibroblast matrices

Matrices were prepared using either dermal of lymphatic fibroblasts and fixed for 20 minutes in buffer containing 4% paraformaldehyde and 4g/ml Sucrose. Matrices were stained for fibronectin as described above and imaged using Leica SP5 II Confocal System. Samples were imaged with 63× objective at 2× zoom power and each z-stack was 0.5μM thick. Stacks were added until fibers were indiscernible and at least 9 measurements were taken for each sample. Images were analyzed using ImageJ Plugin OrientationJ (available for download at http://bigwww.epfl.ch/demo/orientation). Images were normalized for orientation using R and graphed. Source code for R used in these analyses has been previously published (13).

2-Photon Microscopy

Inguinal lymph nodes were collected from C57/BL6 mice, held in buffer solution under nylon mesh and imaged with a Leica TCS SP8 MP 2-photon intravital microscope (Leica Microsystems, Inc, Buffalo Grove, IL). The specific region of interest was the lymph node capsule. Collagen was visualized using second harmonic generation (SHG) from 900nm excitation in a Chameleon XR Ti:Saphire laser (Coherent, Inc., Santa Clara, CA). SHG emission was captured in 12 bits, at 700 Hz, through a 25×/1.00 water immersion objective in reflected mode using a HyD detector with a standard DAPI filter set. Mouse tissue images shown are composites of 15 z-stacks with 10mm step size. The images were further processed using Huygens Professional Deconvolution software (Scientific Volume Imaging, B.V., The Netherlands).

Transswell permeability assay

Fibroblast matrices were prepared as described above in 24 well transwell plate (Costar, #3413). 0.2×10^5 fibroblasts were seeded and treated for 5 days with L-ascorbic acid. Following treatment, fibroblasts were lysed with extraction buffer (0.5% Triton X-100, 2mM NH_4OH in DPBS) for 5 minutes at 37°C, 5% CO_2, followed by 1:1 dilution with DPBS and incubated overnight at 4°C. Next day, wells were washed and seeded with endothelial cells at 1×10^5 cells per transwell and incubated at 37°C, 5% CO_2 for 36 hours. Media was collected from the wells, followed by 2 washes with DPBS. Next, 200μl of 2mg/ml dextran red (#R9379, Sigma Aldrich) solution was prepared in HBSS (without phenol red) containing 5% FCS in the upper chamber and 450μl of 5% FCS in HBSS solution was added to the bottom chamber. 50μl sample was collected from the wells at various time intervals and analyzed on EnVision multi-label microplate reader at The Wistar Institute Molecular Screening and Protein Expression Facility. Samples were normalized to blank and graphed.

Melanoma cell migration in organotypic culture (reconstruct)

Cultures were prepared using a modified approach as previously described(29). Cultures were prepared in a 4 well 35mm glass bottom dish for optimal imaging (Greiner cellview #50590467, Thermofisher Scientific). An acellular bottom layer of collagen matrix (1.6ml 10xEMEM [12-684F, Lonza], 0.16ml L-glutamine, 1.82ml heat inactivated FCS, 0.2ml NaHCO3 [17-613E, Lonza], 14.8ml Rat Tail Collagen I [final concentration 1.0mg/ml, #354249, Corning] was added in the dish and allowed to solidify for 1 hour. Next, fibroblasts (6×10^4 cells) were harvested and mixed with 250μl collagen matrix and allowed to set for 1 hour at 37°C. Next, HUVEC (1×10^5 cells) labeled with mCherry were added on the fibroblast layer and incubated for 48 hours at 37°C, 5% CO_2. Next, 1205lu melanoma cells labeled with GFP were plated at 1×10^5 cells per well and incubated in media prepared with 1:1 ratio of EGM-2MV and DMEM 10% FCS. The following day, time-lapse images were acquired on a Leica TCS SP8 X WLL Scanning Confocal Microscope. Image deconvolution was performed using Huygens Professional and analyzed using NIS Elements Advanced software and graphed using Graphpad/Prism6.

In vivo xenograft assay

All animal experiments were approved by the Institutional Animal Care and Use Committee (IACUC) (IACUC #112503X_0) and were performed in an Association for the Assessment and Accreditation of Laboratory Animal Care (AAALAC) accredited facility. YUMM1.7 (1×10^5 cells) overexpressing mCherry were injected subcutaneously into aged (50 weeks) and young (8 weeks) C57/BL6 mice (#556, Charles River). Mice were treated as follows with rHAPLN1 (100 ng into the inguinal lymph node, #2608-HP, R&D Systems, twice weekly) or PBS as control, starting two weeks prior to tumor injection and continuing until sacrifice. Tumor sizes were measured every 3-4 days using digital calipers, and tumor volumes were calculated using the following formula: volume = $0.5 \times$ (length $\times$ width^2). Time-to-event (survival) was determined by a 5-fold increase in baseline volume (~1000 mm^3) and was limited by the development of skin necrosis. Mice were euthanized, lungs and lymph nodes were harvested and metastases counted. Half of the tissue was embedded in paraffin and half in optimal cutting temperature compound (O.C.T, Sakura, Japan City) and flash frozen for

sectioning. Lungs and lymph nodes were sectioned and stained with mCherry (NBP2-25157, Novus Biologicals) to determine melanoma metastasis. All reagents injected in live mice were tested for endotoxin levels at University of Pennsylvania Cell Center Services using The Associates of Cape Cod LAL test.

TCGA database analysis

The RNAseq and Clinical dataset for skin cutaneous melanoma (30) was downloaded from The Cancer Genome Atlas (TCGA; http://cancergenome.nih.gov/). Normalized mRNA expression was analyzed by quartiles. Patient ages were grouped into categories (50, 51-79, and 80 years).

Gene Set Expression Analysis

We performed a targeted analysis on GSEA gene signatures related to ECM organization. GO ECM fibril organization gene signature was downloaded from Molecular Signatures Database (http://software.broadinstitute.org/gsea/msigdb/index.jsp). GSEA analysis was performed using javaGSEA desktop application available from http://software.broadinstitute.org/gsea/downloads.jsp. TCGA samples that were processed from regional lymph node metastases were used in GSEA analysis. For these LN samples, the GSEA score matrix was organized as having samples in the column and signature genes in the rows. Any sample that did not include either patient age or did not have associated gene expression data for the sample was excluded in the analysis. Differentially enriched signatures were defined as having nominal p-value below 0.05 and FDR below 5%.

Statistical analyses

For in vitro studies, a Student t test or Wilcoxon rank-sum test (Mann–Whitney) was performed for two-group comparison. Estimate of variance was performed, and parameters for the t test were adjusted accordingly using Welch's correction. ANOVA or Kruskal–Wallis test with post-hoc Bonferroni's or Holm–Sidak's adjusted P values was used for multiple comparisons. For in vivo studies, repeated measures ANOVA was calculated between samples. The Holm–Sidak correction was performed. For other experiments, Graphpad/Prism6 was used for plotting graphs and statistical analysis. Survival analyses included Kaplan-Meier log rank test and multivariable Cox regression for univariate and multivariate analyses, respectively. Data was represented as ±SEM. Significance was designated as follows: *, $P < 0.05$; **, $P < 0.01$; and ***, $P < 0.001$.

Supplementary Material

Refer to Web version on PubMed Central for supplementary material.

Acknowledgments

Abbreviations:

HAPLN1	hyaluronan and proteoglycan link protein 1
LN	Lymph Node
SNB	Sentinel Lymph Node Biopsy
ECM	Extracellular Matrix
AJCC	American Joint Committee on Cancer
DMFS	Distant Metastasis Free Survival
HUVEC	human umbilical vascular endothelial cells

References:

1. Balch CM, Soong SJ, Gershenwald JE, Thompson JF, Reintgen DS, Cascinelli N, et al. Prognostic factors analysis of 17,600 melanoma patients: validation of the American Joint Committee on Cancer melanoma staging system. J Clin Oncol. 2001;19:3622–34. [PubMed: 11504744]

2. Amin MB, Greene FL, Edge SB, Compton CC, Gershenwald JE, Brookland RK, et al. The Eighth Edition AJCC Cancer Staging Manual: Continuing to build a bridge from a population-based to a more "personalized" approach to cancer staging. CA Cancer J Clin. 2017;67:93–9. [PubMed: 28094848]

3. Balch CM, Soong SJ, Gershenwald JE, Thompson JF, Coit DG, Atkins MB, et al. Age as a prognostic factor in patients with localized melanoma and regional metastases. Ann Surg Oncol. 2013;20:3961–8. [PubMed: 23838920]

4. Lasithiotakis K, Leiter U, Meier F, Eigentler T, Metzler G, Moehrle M, et al. Age and gender are significant independent predictors of survival in primary cutaneous melanoma. Cancer. 2008;112:1795–804. [PubMed: 18306371]

5. Morton DL. Overview and update of the phase III Multicenter Selective Lymphadenectomy Trials (MSLT-I and MSLT-II) in melanoma. Clin Exp Metastasis. 2012;29:699–706. [PubMed: 22729520]

6. Wissmann C, Detmar M. Pathways targeting tumor lymphangiogenesis. Clin Cancer Res. 2006;12:6865–8. [PubMed: 17145802]

7. Faries MB, Thompson JF, Cochran AJ, Andtbacka RH, Mozzillo N, Zager JS, et al. Completion Dissection or Observation for Sentinel-Node Metastasis in Melanoma. N Engl J Med. 2017;376:2211–22. [PubMed: 28591523]

8. Page AJ, Li A, Hestley A, Murray D, Carlson GW, Delman KA. Increasing Age Is Associated with Worse Prognostic Factors and Increased Distant Recurrences despite Fewer Sentinel Lymph Node Positives in Melanoma. Int J Surg Oncol. 2012;2012:456987. [PubMed: 22523678]

9. Chao C, Martin RC, 2nd, Ross MI, Reintgen DS, Edwards MJ, Noyes RD, et al. Correlation between prognostic factors and increasing age in melanoma. Ann Surg Oncol. 2004;11:259–64. [PubMed: 14993020]

10. Kang JS, Kawakami Y, Bekku Y, Ninomiya Y, Izpisua Belmonte JC, Oohashi T. Molecular cloning and developmental expression of a hyaluronan and proteoglycan link protein gene, crtl1/hapln1, in zebrafish. Zoological science. 2008;25:912–8. [PubMed: 19267601]

11. Huang-Lee LL, Nimni ME. Crosslinked CNBr-activated hyaluronan-collagen matrices: effects on fibroblast contraction. Matrix Biol. 1994;14:147–57. [PubMed: 8061927]

12. Karjalainen JM, Tammi RH, Tammi MI, Eskelinen MJ, Agren UM, Parkkinen JJ, et al. Reduced level of CD44 and hyaluronan associated with unfavorable prognosis in clinical stage I cutaneous melanoma. Am J Pathol. 2000;157:957–65. [PubMed: 10980134]

Author Manuscript

13. Kaur A, Ecker BL, Douglass SM.,Kugel CH, 3rd, Webster MR., Almeida FV., et al. Remodeling of the collagen matrix in aging skin promotes melanoma metastasis and affects immune cell motility. Cancer Discovery. 2018;In Press.

14. Roozendaal R, Mebius RE, Kraal G. The conduit system of the lymph node. Int Immunol. 2008;20:1483–7. [PubMed: 18824503]

15. Zolla V, Nizamutdinova IT, Scharf B, Clement CC, Maejima D, Akl T, et al. Aging-related anatomical and biochemical changes in lymphatic collectors impair lymph transport, fluid homeostasis, and pathogen clearance. Aging Cell. 2015;14:582–94. [PubMed: 25982749]

16. Karaman S, Buschle D, Luciani P, Leroux JC, Detmar M, Proulx ST. Decline of lymphatic vessel density and function in murine skin during aging. Angiogenesis. 2015;18:489–98. [PubMed: 26260189]

17. Dankort D, Curley DP, Cartlidge RA, Nelson B, Karnezis AN, Damsky WE, Jr., et al. Braf(V600E) cooperates with Pten loss to induce metastatic melanoma. Nat Genet. 2009;41:544–52. [PubMed: 19282848]

18. Nathanson SD. Insights into the mechanisms of lymph node metastasis. Cancer. 2003;98:413–23. [PubMed: 12872364]

19. Vega F, Coombes KR, Thomazy VA, Patel K, Lang W, Jones D. Tissue-specific function of lymph node fibroblastic reticulum cells. Pathobiology. 2006;73:71–81. [PubMed: 16943687]

20. Giannotta M, Trani M, Dejana E. VE-cadherin and endothelial adherens junctions: active guardians of vascular integrity. Dev Cell. 2013;26:441–54. [PubMed: 24044891]

21. Baluk P, McDonald DM. Markers for microscopic imaging of lymphangiogenesis and angiogenesis. Ann N Y Acad Sci. 2008;1131:1–12. [PubMed: 18519955]

22. Podgrabinska S, Skobe M. Role of lymphatic vasculature in regional and distant metastases. Microvasc Res. 2014;95:46–52. [PubMed: 25026412]

23. Patel JK, Didolkar MS, Pickren JW, Moore RH. Metastatic pattern of malignant melanoma. A study of 216 autopsy cases. Am J Surg. 1978;135:807–10. [PubMed: 665907]

24. Leong SP, Cady B, Jablons DM, Garcia-Aguilar J, Reintgen D, Jakub J, et al. Clinical patterns of metastasis. Cancer Metastasis Rev. 2006;25:221–32. [PubMed: 16770534]

25. Morton DL, Thompson JF, Cochran AJ, Mozzillo N, Nieweg OE, Roses DF, et al. Final trial report of sentinel-node biopsy versus nodal observation in melanoma. N Engl J Med. 2014;370:599–609. [PubMed: 24521106]

26. Kaur A, Webster MR, Marchbank K, Behera R, Ndoye A, Kugel CH, 3rd, et al. sFRP2 in the aged microenvironment drives melanoma metastasis and therapy resistance. Nature. 2016;532:250–4. [PubMed: 27042933]

27. Siamakpour-Reihani S, Caster J, Bandhu Nepal D, Courtwright A, Hilliard E, Usary J, et al. The role of calcineurin/NFAT in SFRP2 induced angiogenesis--a rationale for breast cancer treatment with the calcineurin inhibitor tacrolimus. PLoS One. 2011;6:e20412. [PubMed: 21673995]

28. Franco-Barraza J, Beacham DA, Amatangelo MD, Cukierman E. Preparation of Extracellular Matrices Produced by Cultured and Primary Fibroblasts. Curr Protoc Cell Biol. 2016;71:1091–934.

29. Berencsi K, Meropol NJ, Hoffman JP, Sigurdson E, Giles L, Rani P, et al. Colon carcinoma cells induce CXCL11-dependent migration of CXCR3-expressing cytotoxic T lymphocytes in organotypic culture. Cancer Immunol Immunother. 2007;56:359–70. [PubMed: 16783574]

30. Cancer Genome Atlas N Genomic Classification of Cutaneous Melanoma. Cell. 2015;161:1681–96. [PubMed: 26091043]

Significance:

Our studies reveal that changes in the stroma during aging may influence the way tumor cells traffic through the lymphatic vasculature. Aging may dictate the route of metastatic dissemination of tumor cells, and understanding these changes may help to reveal targetable moieties in the aging tumor microenvironment.
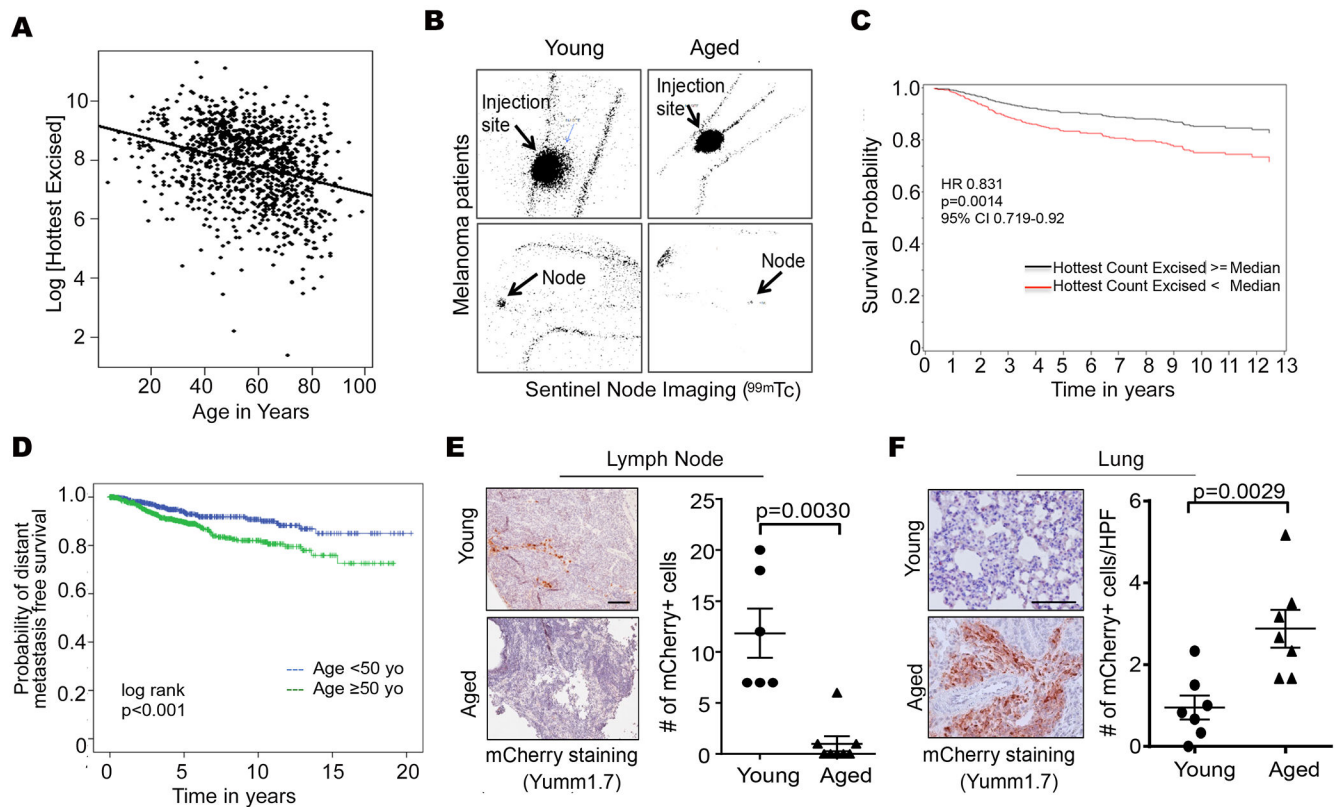
Figure 1. Retention of technicium dye and patterns of metastatic dissemination correlate with age.

A. Consecutive melanoma patients (n=1081) were injected with ^{99m}Tc sulfur colloid in the region of the primary tumor and a gamma probe was used to quantify the signal intensity in the surgically resected sentinel lymph node (Spearman's ρ=−0.30, p<0.001) B. Representative lymphoscintigraphy of Tc-99m sulfur colloid signal in young and aged melanoma patients; C. Survival curve adjusted for #of positive SLN, T-stage and ulceration, stratified by hottest counts above or below the median (HR 0.831, p=0.0014 95% CI 0.719-0.92); D. Kaplan-Meier analysis of distant metastatic-free survival in sentinel lymph node biopsy negative patients, stratified by patient age at diagnosis (n=1,649; log rank p<0.001); E. mCherry-labeled Yumm1.7 cells were injected into young or aged C57BL/6 mice and metastatic cells were identified in the draining inguinal lymph node by immunohistochemistry (bar=100μm). Number of cells were counted per lymph node and graphed (two-tailed unpaired t-test, p=0.0030); F. The mean number of metastases per high power field was similarly determined for lungs from the matching young and aged C57BL/6 mouse cohort (two-tailed unpaired t-test, p=0.0029).
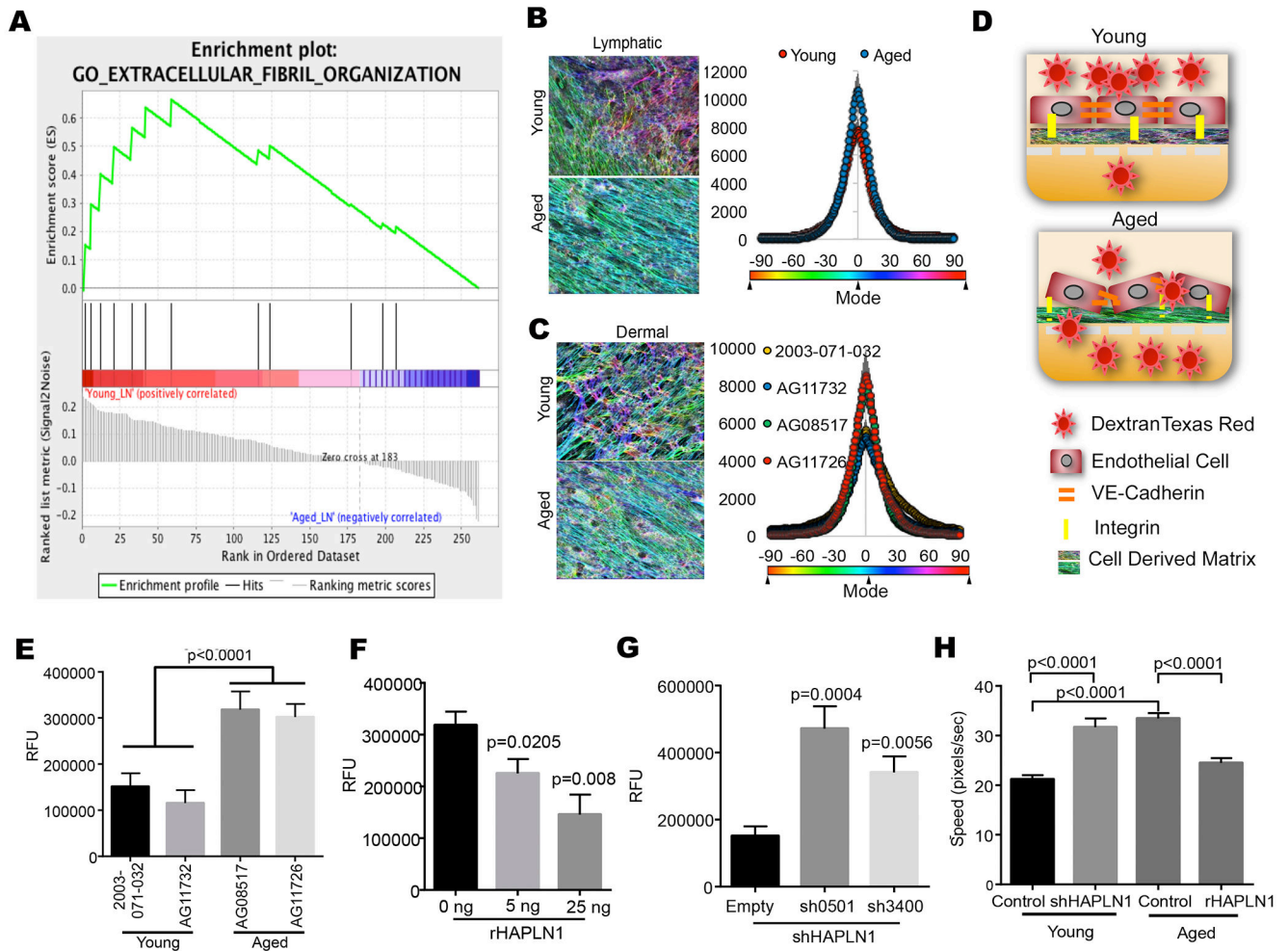
Figure 2. Changes in lymphatic fibroblast ECM deposition according to age.

A. GSEA analysis for ECM fibril organization of lymph nodes from human melanoma patients (n=221; nominal p=0.008); B. *In vitro* extracellular matrix was produced by lymphatic fibroblasts isolated from young and aged donors and analyzed for the levels of fiber orientation by fibronectin immunofluorescence. The fiber distribution was determined by calculating the percent of fibers arranged in parallel for each acquired region (± 90° of the mode angle); each point in the corresponding dotplot represent the mean number of fibers orientated at each angle (paired bars represent the standard error of the mean); C. Analysis of extracellular matrix orientation produced *in vitro* by dermal fibroblasts from young or aged healthy donors; D. Schematic of experimental setup: Matrices derived from young and aged fibroblasts were reconstituted with HUVECs followed by incubation with Texas red dye in the upper transwell chamber. Permeability was determined by quantification of the fluorescence of the lower chamber after 30 minutes. E, Permeability of endothelial cells plated on young and aged matrices as measured by Texas red (two-tailed unpaired t-test: young vs. aged, p<0.001); F. Transwell permeability assay of HUVECs plated on acellular extracellular matrices produced by extracted aged fibroblasts treated with increasing doses of rHAPLN1 (ANOVA p=0.0032; two-tailed unpaired t-test: 0 ng vs. 5 ng,

p=0.0205; 0 ng vs. 25 ng, p=0.0080); G. Transwell permeability assay of HUVECs plated on acellular extracellular matrices produced by extracted young fibroblasts with shHAPLN1 knockdown (ANOVA p=0.0004; two-tailed unpaired t-test: shempty vs. sh0501, p=0.0004; shempty vs. sh3400, p=0.0056); H. Quantification of GFP-labeled melanoma cell migration (48 hours) on cell derived matrices under different conditions (ANOVA p=0.0004; all pairwise comparisons by two-tailed t-tests, p<0.001).
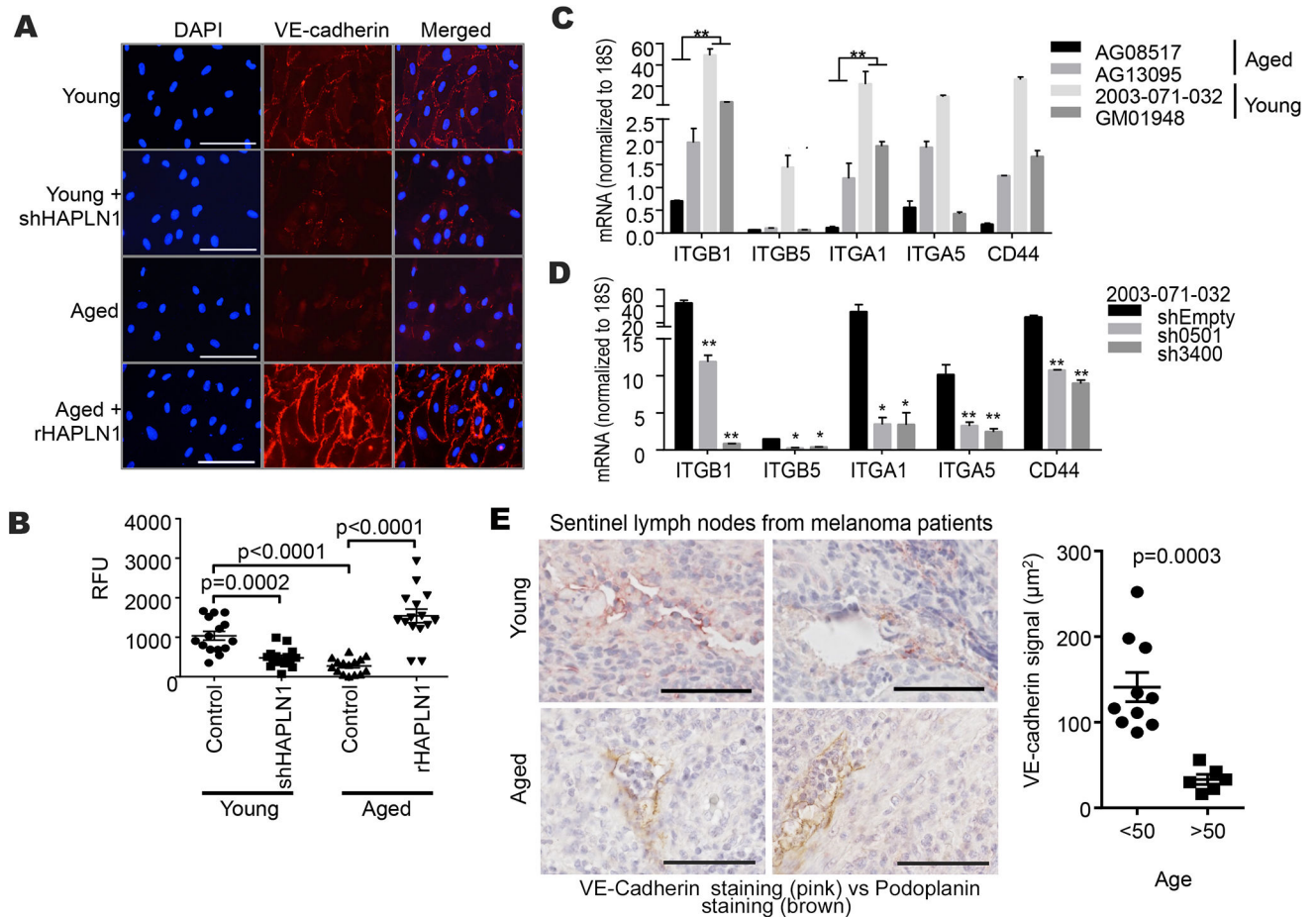
Figure 3. Changes in cell-adhesion and integrin expression with age.
A. Representative VE-cadherin (red) confocal immunofluorescence of HUVECs plated on acellular matrices following extraction of young shEmpty and shHAPLN1 fibroblasts and aged fibroblasts treated with rHAPLN1 (25 ng/mL) or PBS (bar=100μm); B. Corresponding quantification of the signal intensity of VE-cadherin positive cellular adhesions between HUVECs; C. Relative expression by qtPCR of integrins (ITGB1, ITGB5, IGTA1, ITGA5) and CD44 of HUVECs on acellular matrices produced by young or aged fibroblasts (** p<0.01); D. Relative expression by qtPCR of integrins (ITGB1, ITGB5, IGTA1, ITGA5) and CD44 of HUVECs on acellular matrices produced by young fibroblasts following HAPLN1 knockdown (* p<0.05; ** p<0.01); E. Representative podoplanin (brown) and VE-cadherin (red) two-color immunohistochemistry of human sentinel lymph node specimens from primary cutaneous melanoma patients (n=16; bar=100μm); F. VE-cadherin signal quantification from human sentinel lymph nodes (n=16; two-tailed unpaired t-test, p=0.0003).
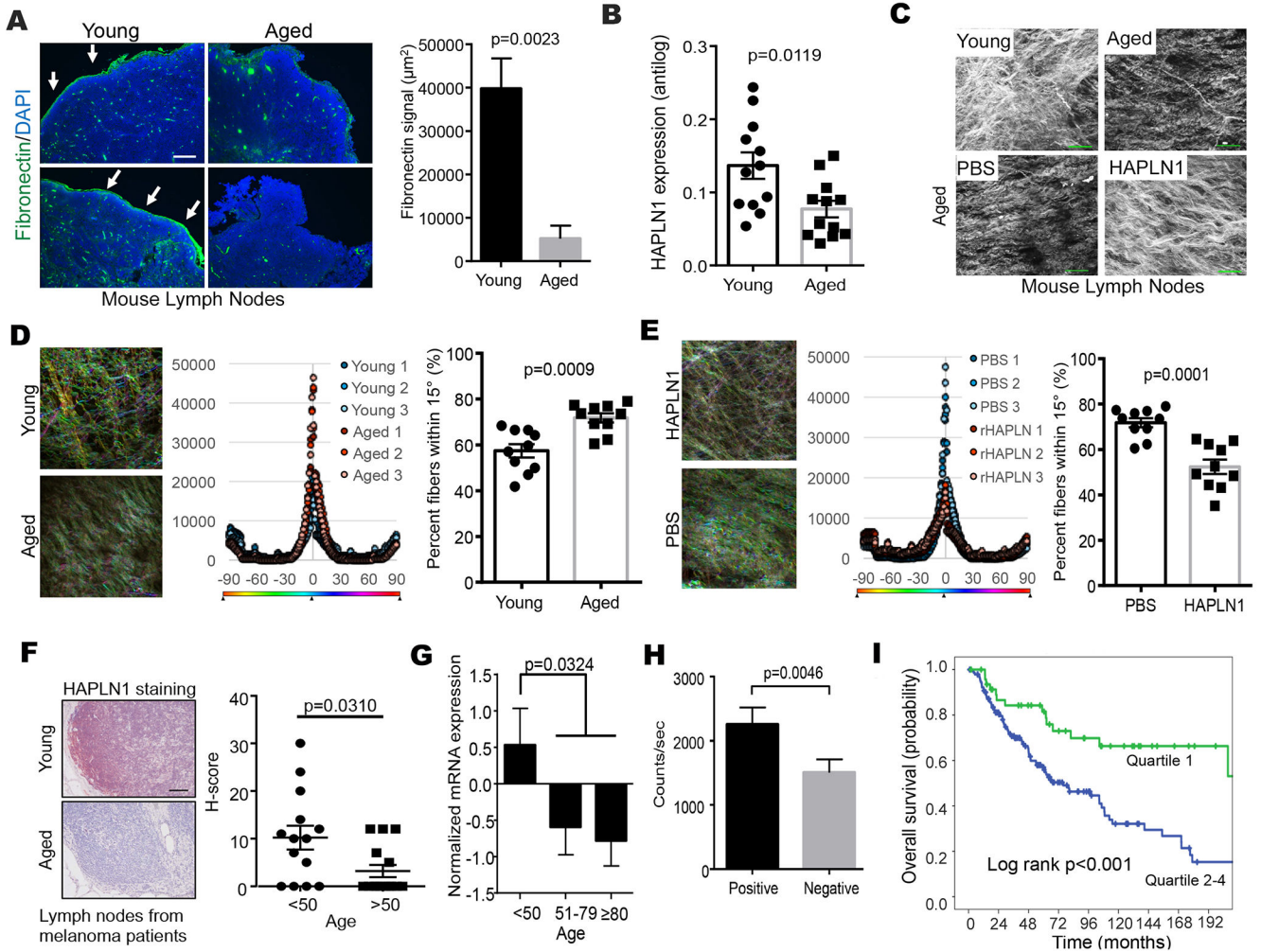
Figure 4. Effects of HAPLN1 on lymph node integrity.
A. Representative two-photon microscopy of pericapsular collagen structure of inguinal lymph node in young or aged C57BL/6 mice, and corresponding quantification; B, HAPLN1 mRNA expression as measured by RT-PCR. C. Representative two-photon microscopy of pericapsular collagen structure of inguinal lymph node in aged C57BL/6 mice treated with rHAPLN1 (100 ng twice weekly) or PBS; D. Quantification of young and aged lymphatic pericapsular extracellular matrix fiber orientation by collagen fluorescence. Each point in the corresponding dotplot represent the mean number of fibers orientated at each angle (paired bars represent the standard error of the mean). The fiber distribution was determined by calculating the percent of fibers arranged in parallel for each acquired region (±90° of the mode angle); the percent of fibers within 15° of the mode was compared between study arms (two-tailed unpaired t-test, p=0.0009); E. Quantification of lymphatic pericapsular extracellular matrix fiber orientation by collagen fluorescence after HAPLN1 treatment; F. Representative HAPLN1 immunohistochemistry of sentinel lymph node specimens of clinically node-negative melanoma patients (bar=100μm). Each sample was assigned a H-score that included the relative signal intensity and area of staining (n=30; two-tailed unpaired t-test, p=0.0310); G. Age-stratified TCGA analysis of HAPLN1 mRNA expression

in regional lymphatic tissue of primary melanoma patients (n=192; two-tailed unpaired t-test, p=0.0324); H. Geiger counts of melanoma patients following sentinel lymph node biopsy with Tc-99m sulfur colloid injection, stratified by HAPLN1-positivity by immunohistochemistry staining (n=86; two-tailed unpaired t-test, p=0.0046); I. Kaplan-Meier survival function of non-metastatic human melanoma patients in the TCGA database, stratified by quartiles of regional lymph node HAPLN1 mRNA (n=192; log rank p<0.001).
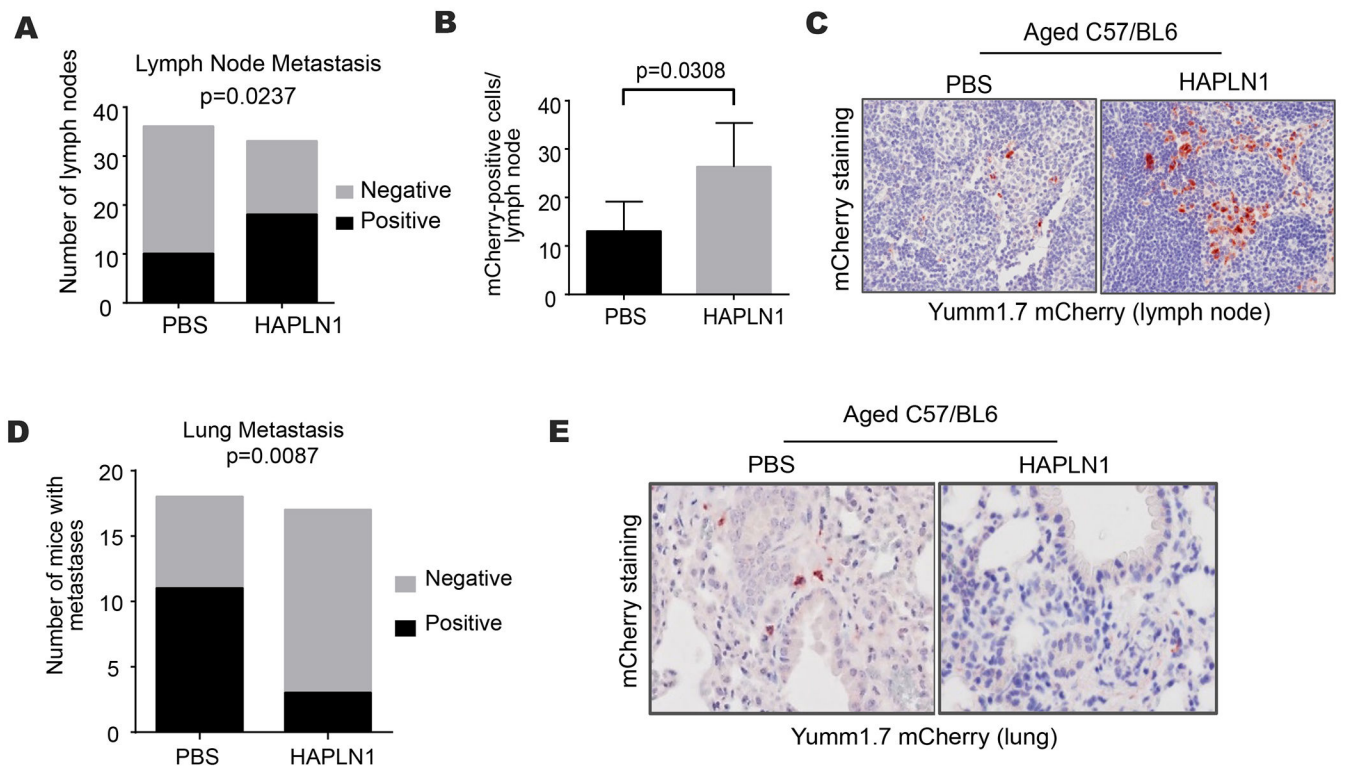
Figure 5. In vivo effects of HAPLN1 on routes of metastatic dissemination.
A. mCherry-labeled yumm 1.7 cells were injected into aged C57BL/6 mice (n=18/arm) and the draining lymph nodes were treated with HAPLN1 (100 ng) or PBS. Tumor metastasis in the draining lymphatics were identified by immunohistochemical staining (chi squared p=0.0237); B. Lymphatic tumor burden was quantified (two-tailed unpaired t-test, p=0.0308); C. Representative immunohistochemistry of mCherry-positive metastasis (red) in draining lymphatics; D. Tumor metastasis in the lung in the identical mouse cohort were identified by immunohistochemical staining (chi squared p=0.0087); E. Representative immunohistochemistry of mCherry-positive metastasis (red) in the lungs.
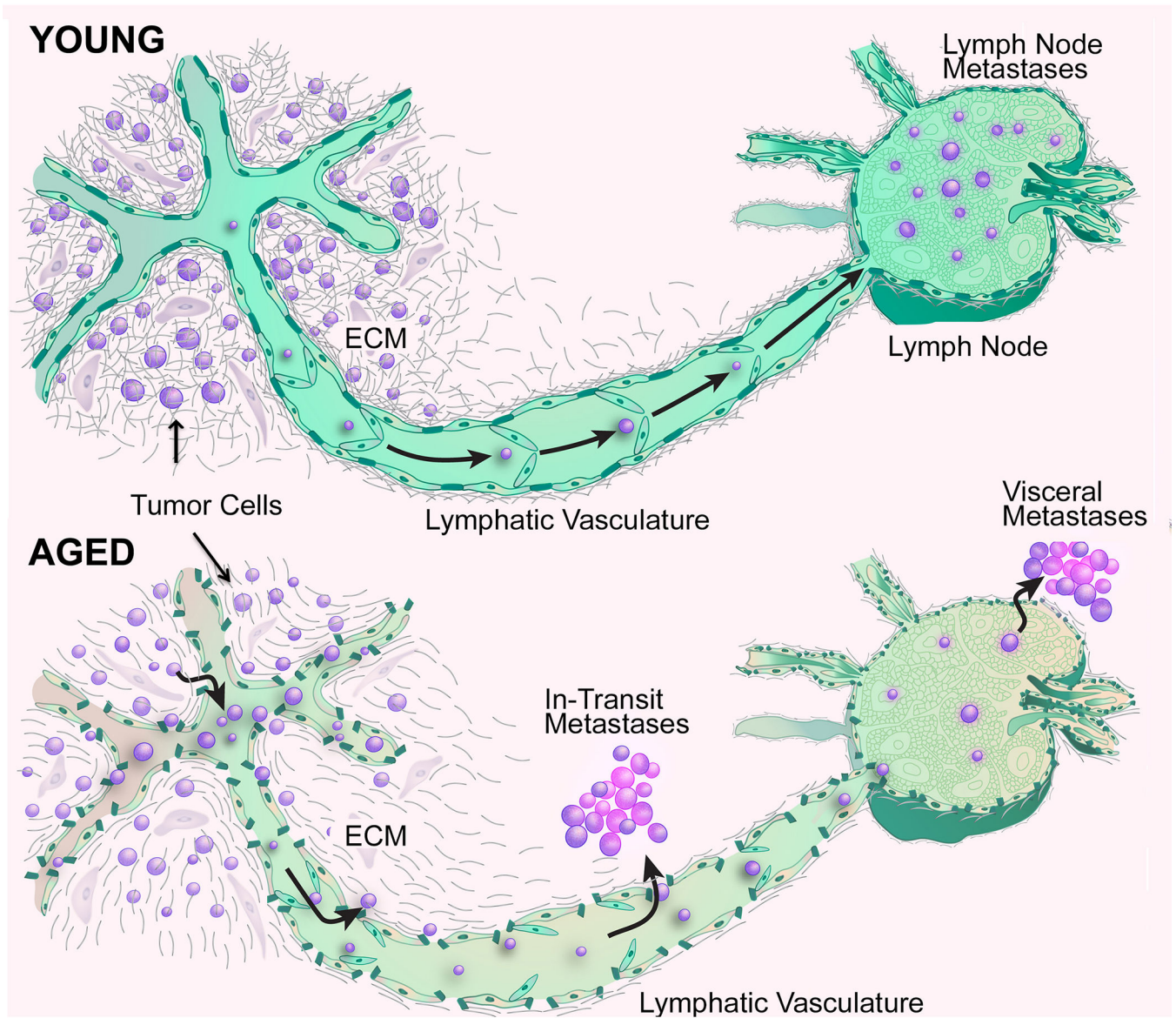
Figure 6. Schematic representation of age-dependent changes in melanoma tumor progression.
Age-related changes in the peri-lymphatic stroma impair the integrity of lymphatic vessels and nodes and increase lymphatic permeability. Such differences may underlie the clinical observations of increased rates of in-transit disease and false negative sentinel lymph node biopsies.

Table 1.

Cox proportional hazards model evaluating the impact of HAPLN1 expression on overall survival, accounting for pathologic stage and patient age.

		HR*	95% CI	p-value
AJCC Pathologic stage	I	Ref	Ref	0.001
	II	1.68	0.93-3.06	0.088
	III	2.70	1.62-4.53	<0.001
Age, years (increasing)		**1.02**	**1.01-1.04**	**0.002**
HAPLN1	*Q2-4*	*Ref*	*Ref*	*0.004*
	Q1	*0.44*	*0.25-0.77*	

*
Hazard ratio (HR) indicates relative hazard for death and was adjusted for all variables included